Capturing microscopic features of bone remodeling into a macroscopic model based on biological rationales of bone adaptation

AUTHOR(S):

Kim, Kwan Young; Kameo, Yoshitaka; Tanaka, Sakae; Adachi, Taiji

Capturing microscopic features of bone remodeling into a macroscopic model based on biological rationales of bone adaptation

Young Kwan Kim[a, b], Yoshitaka Kameo[b], Sakae Tanaka[a], Taiji Adachi[b]

a: Department of Orthopaedic Surgery, Faculty of Medicine, The University of Tokyo
b: Department of Biosystems Science, Institute for Frontier Life and Medical Sciences, Kyoto University

Corresponding author:	Taiji Adachi, Ph.D.
Mailing Address:	Department of Biosystems Science
	Institute for Frontier Life and Medical Sciences
	Kyoto University
	53 Kawahara-cho, Shogoin, Sakyo-ku, Kyoto, 606-8507, Japan
Telephone:	+81-75-751-4853
Fax:	+81-75-751-4853
E-mail:	adachi@frontier.kyoto-u.ac.jp

Abstract

To understand Wolff's law, bone adaptation by remodeling at the cellular and tissue levels has been discussed extensively through experimental and simulation studies. For the clinical application of a bone remodeling simulation, it is significant to establish a macroscopic model that incorporates clarified microscopic mechanisms. In this study, we proposed novel macroscopic models based on the microscopic mechanism of osteocytic mechanosensing, in which the flow of fluid in the lacuno-canalicular porosity generated by fluid pressure gradients plays an important role, and theoretically evaluated the proposed models, taking biological rationales of bone adaptation into account. The proposed models were categorized into two groups according to whether the remodeling equilibrium state was defined globally or locally, i.e., the global or local uniformity models. Each remodeling stimulus in the proposed models was quantitatively evaluated through image-based finite element analyses of a swine cancellous bone, according to two introduced criteria associated with the trabecular volume and orientation at remodeling equilibrium based on biological rationales. The evaluation suggested that nonuniformity of the mean stress gradient in the local uniformity model, one of the proposed stimuli, has high validity. Furthermore, the adaptive potential of each stimulus was discussed based on spatial distribution of a remodeling stimulus on the trabecular surface. The theoretical consideration of a remodeling stimulus based on biological rationales of bone adaptation would contribute to the establishment of a clinically applicable and reliable simulation model of bone remodeling.

Keywords

Bone adaptation, Wolff's law, Biological rationale, Model reduction, Multiscale biomechanics, Mechanobiology

1 Introduction

The bone structure undergoes remodeling to adapt to the mechanical environment. As such, Wolff proposed a law of bone transformation, known as Wolff's law, which describes the mathematical correspondence between trabecular architecture and principal stress trajectories (Wolff 1869, 1892). This law represents the biological features of bone adaptation from a macroscopic viewpoint. To improve biomechanical understanding of bone adaptation by remodeling, mathematical modeling and simulation by computational approaches, including finite element analysis, have been developed as quite useful methods.

Macroscopic models of bone remodeling that assume a remodeling stimulus to be a macroscopic mechanical quantity such as stress, stress nonuniformity, strain, or strain energy density, have been proposed (Cowin and Hegedus 1976; Carter 1984; Carter et al. 1987; Huiskes et al. 1987; van Rietbergen et al. 1995; Adachi et al. 1997; Huiskes et al. 2000; Adachi et al. 2001; Ruimerman et al. 2005). In these models, cancellous bone resorption and formation are described by volume change or trabecular surface movement, according to values of macroscopic mechanical stimuli. These macroscopic models have been demonstrated to be of practical importance clinically, such as in designing bone tissue engineering scaffolds (Adachi et al. 2006; Lacroix et al. 2006) and prostheses for joint replacement (Sharma et al. 2010) and predicting the clinical outcome of callus distraction (Reina-Romo et al. 2011) and orthodontic tooth movement (Hasegawa et al. 2015).

Microscopic mechanisms of bone remodeling have also been studied extensively. Osteocytes are known to be responsible for the regulation of osteoclastic bone resorption and osteoblastic bone formation by sensing mechanical stimuli and communicating with the effector cells through their

complex intercellular network (Aarden et al. 1994; Burger and Klein-Nulend 1999). This osteocytic mechanosensing is believed to be triggered by interstitial fluid flow in the lacuno-canalicular system, which is generated by a fluid pressure gradient (Weinbaum et al. 1994; Cowin et al. 1995; Han et al. 2004; Temiyasathit and Jacobs 2010). This mechanism has been the basis for the proposed microscopic remodeling models, which regard bone tissue as a poroelastic structure and take into account the osteocytic sensation of load-induced fluid flow stimuli (Swan et al. 2003; Adachi et al. 2010; Kumar et al. 2011; Kameo and Adachi 2014a, b). These models, which have shown that load-induced fluid flow stimuli can drive bone remodeling, have expanded the frontiers of microscopic biomechanics of bone adaptation.

Clinical applications of computational bone remodeling simulations require macroscopic models that can predict biological behaviors because of their low computational cost in solving large-scale clinical problems. The construction of clinically applicable and reliable macroscopic models requires the integration of microscopic mechanisms into the macroscopic models. However, incorporating more details on clarified microscopic mechanisms of bone remodeling into a macroscopic model increases the degrees of freedom (DOF) thereof, which can impose large computational costs. One possible approach to overcome this problem is the reduction of the model's DOF, through which essential features are captured from detailed microscopic mechanisms and incorporated into a simple macroscopic model. The reduced macroscopic model should be carefully examined for its potential to express the biological nature of bone adaptation. It is crucial, therefore, to construct macroscopic models based on biological rationales.

The purpose of this study is to propose novel macroscopic models of bone remodeling that

incorporate the microscopic mechanism of osteocytic mechanosensing and to theoretically evaluate the proposed models, taking biological rationales into account. The models assume possible remodeling stimuli based on two mechanical quantities (the mean stress or the mean stress gradient), which reflect the microscopic mechanism. The proposed remodeling stimuli were categorized into two groups according to whether the remodeling equilibrium state is defined globally or locally: the global and local uniformity models. Through image-based finite element analyses of a swine cancellous bone, each remodeling stimulus in the proposed models was quantitatively evaluated according to two introduced criteria associated with the trabecular volume and orientation based on biological rationales. The evaluation suggested that nonuniformity of the mean stress gradient in the local model has high validity. Furthermore, to discuss the adaptive potential of each model, spatial distribution of a remodeling stimulus on the trabecular surface was visualized.

2 Methods

2.1 The mathematical model of trabecular bone remodeling

The mathematical models in this study assumed that bone remodeling is driven toward achieving uniformity of a mechanical quantity on the trabecular surface. The proposed models were categorized into two groups, i.e., the global and local uniformity models, according to whether the remodeling equilibrium state is defined globally or locally. In the global uniformity models, as shown in Fig. 1(a), a remodeling stimulus S_{sf} on the trabecular surface is defined as a mechanical quantity q in itself at a point on the trabecular surface, while bone remodeling is driven by referring to the equilibrium value $S_{\mathrm{sf}}^{\mathrm{o}}$ that is globally set by $S_{\mathrm{sf}}^{\mathrm{o}} = \bar{q}$, which has been empirically determined as a reference value of a

stimulus (Mullender and Huiskes 1995; Ruimerman et al. 2005). However, in the local uniformity models (Adachi et al. 1997; Tsubota et al. 2002; Tsubota and Adachi 2005; Tsubota et al. 2009), as shown in Fig. 1(b), a remodeling stimulus S_{sf} on the trabecular surface is defined as local nonuniformity of a mechanical quantity q at a point on the trabecular surface. The nonuniformity of a mechanical quantity q is quantified by

$$\Gamma(q) = \ln(q_{\mathrm{c}}/q_{\mathrm{d}}), \qquad (1)$$

where q_{c} denotes the mechanical quantity q at position $\boldsymbol{x}_{\mathrm{c}}$ on the trabecular surface and q_{d} denotes the weighted average value of the quantity q over the neighboring surface area A_{L} around the position $\boldsymbol{x}_{\mathrm{c}}$. Bone remodeling is thereby assumed to be driven by local nonuniformity $\Gamma(q)$, while the equilibrium state is locally determined by $\Gamma = 0$, which represents a local uniform state of the mechanical quantity q, i.e., $q_{\mathrm{c}} = q_{\mathrm{d}}$ in Eq. (1). The weighted average for mechanical quantity q_{d} in Eq. (1) is defined by

$$q_{\mathrm{d}} = \int_{A_{\mathrm{L}}} w(l)q(\boldsymbol{x})dA \Big/ \int_{A_{\mathrm{L}}} w(l)dA, \qquad (2)$$

where l denotes the distance between the position $\boldsymbol{x}_{\mathrm{c}}$ and an arbitrary position $\boldsymbol{x}$ on the trabecular surface within the sensing distance l_{L}, $w(l)$ denotes a weighting function that diminishes with distance l, and A denotes the total surface domain of the trabeculae. The domain of integration in Eq. (2) was determined as the trabecular surface area A_{L} within the sensing distance l_{L}, because a fluid stimulus in the trabeculae is dominant when close to the trabecular surface (Kameo et al. 2009; Kameo et al. 2016). This allowed Γ, a remodeling stimulus S_{sf} at position $\boldsymbol{x}_{\mathrm{c}}$, to be locally quantified based on the difference in the mechanical state at position $\boldsymbol{x}_{\mathrm{c}}$ relative to that over the neighboring surface area A_{L}.

To determine morphological changes in the trabeculae resulting from the remodeling stimulus S_{sf},

the rate of surface movement in the direction normal to the surface $\dot{M}(S_{\mathrm{sf}})$ was introduced. As shown in Fig. 1(c), $\dot{M}$ satisfies $\dot{M} < 0$ for $S_{\mathrm{sf}} < S_{\mathrm{sf}}^{\mathrm{o}}$, which represents bone resorption, and $\dot{M} \geq 0$ for $S_{\mathrm{sf}} \geq S_{\mathrm{sf}}^{\mathrm{o}}$, which represents bone formation. In this study, with the remodeling equilibrium value $S_{\mathrm{sf}}^{\mathrm{o}}$ in the global uniformity models, the global $\bar{q}$ was quantified to be the averaged value of q over the entire surface area. The sensing distance l_{L} in the local uniformity models is associated with communication between cells, such as calcium signal propagation through the intercellular network, and is thought to have a value of several hundred micrometers (Xia and Ferrier 1992; Jing et al. 2013). In this paper, the weighting function $w(l)$ was assumed simply to be a linearly decreasing function, while the sensing distance l_{L} was set as 500 μm.

2.2 Remodeling stimuli on the trabecular surface

The proposed models assume four possible remodeling stimuli S_{sf} based on the two mechanical quantities (the mean stress σ_{m} or the mean stress gradient $|\nabla\sigma_{\mathrm{m}}|$). These quantities include essential features (a static pressure or its gradient) that reflect the microscopic mechanism whereby the fluid pressure gradient generates flow (Kufahl and Saha 1990; Adachi et al. 2010; Kameo and Adachi 2014a,b). The models are categorized into two groups, i.e., the global (S_{sf}: the mean stress σ_{m}, the mean stress gradient $|\nabla\sigma_{\mathrm{m}}|$) and local ($S_{\mathrm{sf}}$: nonuniformity of the mean stress $\Gamma(|\sigma_{\mathrm{m}}|)$ uniformity models, nonuniformity of the mean stress gradient $\Gamma(|\nabla\sigma_{\mathrm{m}}|)$). The validity of these four possible remodeling stimuli was theoretically evaluated according to the criteria introduced in the following sections.

2.3 Criteria for quantitatively evaluating the validity of the remodeling stimulus

To ensure that the biological nature of bone adaptation was retained while incorporating the microscopic features, two criteria that any macroscopic remodeling stimulus should meet were introduced in this section. These criteria were based on biological rationales associated with two macroscopic properties of the trabecular structure (volume and orientation) at remodeling equilibrium. The validity of the four possible remodeling stimuli in the proposed models was quantitatively evaluated according to the criteria.

2.3.1 The first criterion associated with the trabecular volume

The first criterion resulted from considering changes in the trabecular volume in the state of remodeling equilibrium. With the rate of the trabecular surface movement $\dot{M}$, as shown in Fig. 1(c), the rate of the net change in trabecular volume $\dot{V}$ is given by

$$\dot{V} = A \int_{S_{\mathrm{sf}}} \dot{M}(S_{\mathrm{sf}}) f(S_{\mathrm{sf}}) dS_{\mathrm{sf}}, \qquad (3)$$

where $f(S_{\mathrm{sf}})$ denotes the distribution function of the remodeling stimulus S_{sf}, as shown in Fig. 2(a), and A denotes the total surface domain of the trabeculae. In the state of remodeling equilibrium, $\dot{V}$ is considered to be negligibly small. Hence, Eq. (3) leads to

$$\int_{S_{\mathrm{sf}}} \dot{M}(S_{\mathrm{sf}}) f(S_{\mathrm{sf}}) dS_{\mathrm{sf}} = 0. \qquad (4)$$

In addition, in the vicinity of the remodeling equilibrium state, $\dot{M}$ can be approximated by a linear function of S_{sf} as

$$\dot{M}(S_{\mathrm{sf}}) = C(S_{\mathrm{sf}} - S_{\mathrm{sf}}^{\mathrm{o}}), \qquad (5)$$

where C $(C > 0)$ is a positive constant coefficient. If Eq. (5) holds, Eq. (4) requires $f(S_{\mathrm{sf}})$ to be symmetric with respect to $S_{\mathrm{sf}} = S_{\mathrm{sf}}^{\mathrm{o}}$ in the vicinity of the remodeling equilibrium state.

Skewness β, which is a measure of the asymmetry of the distribution function of the remodeling stimulus S_{sf} in the vicinity of the remodeling equilibrium state, was therefore introduced as the first criterion (Tsubota and Adachi 2006). Based on the Fisher–Pearson coefficient of skewness (Doane and Seward 2011), this is defined as

$$\beta = \left\{\int_{A'} (S_{\mathrm{sf}} - S_{\mathrm{sf}}^{\mathrm{o}})^3 \, dA/A\right\}/\delta^3, \qquad (6)$$

where A' denotes a subset of the total surface domain A and S_{sf} satisfies $S_{\mathrm{sf}}^{\mathrm{o}} - \delta \leq S_{\mathrm{sf}} \leq S_{\mathrm{sf}}^{\mathrm{o}} + \delta$ in the domain A'. Here δ denotes the averaged deviation of the remodeling stimulus S_{sf} from the equilibrium value $S_{\mathrm{sf}}^{\mathrm{o}}$ and is defined as

$$\delta = \sqrt{\int_A (S_{\mathrm{sf}} - S_{\mathrm{sf}}^{\mathrm{o}})^2 \, dA/A}. \qquad (7)$$

The validity of a remodeling stimulus was evaluated according to the magnitude of the skewness $|\beta|$. As shown in Fig. 2(b), a small value of $|\beta|$, which represents the symmetry of a distribution function $f(S_{\mathrm{sf}})$ in the vicinity of the remodeling equilibrium state $(S_{\mathrm{sf}}^{\mathrm{o}} - \delta \leq S_{\mathrm{sf}} \leq S_{\mathrm{sf}}^{\mathrm{o}} + \delta)$, ensures the validity of the remodeling stimulus S_{sf} that satisfies Eq. (4).

2.3.2 The second criterion associated with the trabecular orientation

The second criterion was obtained by considering Wolff's law, which assumes that the trabecular orientation corresponds to the principal axes of stress in the remodeling equilibrium state. As depicted in Fig. 2(c), when the principal stress directions coincide with the principal axes of the adapted bone, both the deviation δ of the remodeling stimulus S_{sf} from the equilibrium value and the magnitude of skewness $|\beta|$ of the distribution of the remodeling stimulus $f(S_{\mathrm{sf}})$ will take their minimum values.

Dependence of the deviation δ and the magnitude of skewness $|\beta|$ on the principal stress

direction was therefore introduced as the second criterion. If δ and $|\beta|$ take their minimum values with the given principal stresses along the principal axes of the trabecular structure, the validity of the remodeling stimulus S_{sf} is ensured.

2.4 A 3D image-based finite element model of cancellous bone

Serial images of the cross section of an adult swine femur were obtained using X-ray micro-computed tomography (inspeXio SMX-90CT plus, SHIMADZU), from which a 3D digital image-based finite element model of cancellous bone was constructed, as shown in Fig. 3(a). The specimen was harvested from the major compressive region in a femoral head, which facilitates reasonable estimation of the stress conditions in the cancellous bone on the assumption that compression is applied vertically to its articular surface. The model was constructed as a cube of 230^3 voxels (2.76^3 mm^3). Each element was a cubic voxel with an edge size of 12.0 μm. The bone was assumed to be an isotropic linear elastic material with Young's modulus E = 20 GPa and Poisson's ratio ν = 0.3. The marrow was assumed to be a cavity, and was not considered in the finite element analyses. To transmit uniform stresses to the cancellous model, the model was surrounded by a homogeneous five-voxel-layer with material properties of E = 2.0 GPa and ν = 0.3, and stresses were applied to the surface of the layer. To exclude the artificial influence arising from the boundary conditions, we focused on the central cube region of 180^3 voxels (2.16^3 mm^3) as the volume of interest.

Assuming that the cancellous model obtained was in a state of remodeling equilibrium, the stress conditions were determined according to the trabecular orientation of the cancellous model. As shown in Fig. 3(b), the fabric ellipsoid (Cowin 1985), which represents the trabecular orientation, was

obtained using the mean intercept length method (Whitehouse 1974). The principal values of the fabric tensor $\boldsymbol{H}$, defined as H_1, H_2, and H_3 in descending order, were given as H_1 = 287 μm, H_2 = 215 μm, and H_3 = 202 μm. Given that the trabecular structure was predominantly orientated along the principal axis corresponding to H_1, the largest compressive stress was assumed to be imposed along the principal axis of H_1, which was set as the z'-axis. The other two principal axes corresponding to H_2 and H_3 were set as the x'-axis and the y'-axis, respectively.

2.5 Evaluation of the validity of the remodeling stimulus

The validity of the four possible remodeling stimuli, i.e., the mean stress σ_{m}, the mean stress gradient $|\nabla\sigma_{\mathrm{m}}|$, nonuniformity of the mean stress $\Gamma(|\sigma_{\mathrm{m}}|)$, and nonuniformity of the mean stress gradient $\Gamma(|\nabla\sigma_{\mathrm{m}}|)$, was quantitatively evaluated according to the two criteria introduced in Section 2.3. Mechanical states of the 3D image-based cancellous model obtained in Section 2.4 were analyzed using a finite element method.

2.5.1 Quantitative evaluation of validity according to the first criterion associated with the trabecular volume

The validity of the remodeling stimuli was evaluated according to the first criterion, i.e., the magnitude of skewness $|\beta|$ in Eq. (6). As shown in Fig. 3(c), uniform compressive stresses of −0.2 MPa along the z'-axis and −0.1 MPa along the x'-axis and y'-axis were applied on the outer surface of the layer surrounding the cancellous model. Assuming the cancellous model to be a representative volume element (RVE), regarded as a continuum, the applied stresses to the model correspond to the

macroscopic stress state with three principal stresses. The magnitude of skewness $|\beta|$ was quantified by Eq. (6), based on the stress distribution obtained by a finite element analysis of the cancellous model. From $|\beta|$, the validity of a remodeling stimulus was compared among all stimuli S_{sf} noted in Section 2.2: σ_{m} and $|\nabla\sigma_{\mathrm{m}}|$ in the global uniformity models and $\Gamma(|\sigma_{\mathrm{m}}|)$ and $\Gamma(|\nabla\sigma_{\mathrm{m}}|)$ in the local uniformity models.

2.5.2 Quantitative evaluation of validity according to the second criterion associated with the trabecular orientation

Further evaluation for the four possible remodeling stimuli was performed according to the second criterion introduced in Subsection *2.3.2*, showing that the deviation δ of the remodeling stimulus S_{sf} from the equilibrium value and the magnitude of skewness $|\beta|$ of the distribution function $f(S_{\mathrm{sf}})$ depend on the principal stress direction. The stresses described in Subsection *2.5.1* were applied to the cancellous model as a reference condition. The direction of the compressive stress along the x'-axis was fixed, whereas the other two principal stress directions were rotated with respect to the x'-axis in a counterclockwise direction, from 0° to 180°, as shown in Fig. 3(d). Angle $\theta_{x'}$ denotes the principal stress direction rotated from the reference condition. The averaged deviation δ of the remodeling stimulus S_{sf} from the equilibrium value $S_{\mathrm{sf}}^{\mathrm{o}}$ and the magnitude of skewness $|\beta|$ of the distribution function $f(S_{\mathrm{sf}})$ were obtained for each stress condition. According to the dependence of δ and $|\beta|$ on the principal stress direction, the validity of a remodeling stimulus was compared among all stimuli S_{sf}: σ_{m}, $|\nabla\sigma_{\mathrm{m}}|$, $\Gamma(|\sigma_{\mathrm{m}}|)$, and $\Gamma(|\nabla\sigma_{\mathrm{m}}|)$.

3 Results

3.1 Quantitative evaluation of validity according to the first criterion associated with the trabecular volume

Figure 4 shows the distribution functions $f(S_{\mathrm{sf}})$ of all four possible remodeling stimuli, i.e., the mean stress σ_{m}, the mean stress gradient $|\nabla\sigma_{\mathrm{m}}|$, nonuniformity of the mean stress $\Gamma(|\sigma_{\mathrm{m}}|)$, and nonuniformity of the mean stress gradient $\Gamma(|\nabla\sigma_{\mathrm{m}}|)$. As shown in Fig. 4(a, c), focusing on models based on the uniformity of the mean stress, σ_{m} and $\Gamma(|\sigma_{\mathrm{m}}|)$ showed almost the same values for the magnitude of skewness ($|\beta|$ = 0.077, 0.076). In contrast, as shown in Fig. 4(b, d), with models based on the uniformity of the mean stress gradient, $|\nabla\sigma_{\mathrm{m}}|$ and $\Gamma(|\nabla\sigma_{\mathrm{m}}|)$ showed quite different values for the magnitude of skewness ($|\beta|$ = 0.433, 0.032), which were the largest and the smallest values among the four remodeling stimuli, respectively. According to the first criterion associated with the trabecular volume, $\Gamma(|\nabla\sigma_{\mathrm{m}}|)$ has the highest validity with the smallest magnitude of skewness $|\beta|$ among the four possible stimuli S_{sf}.

3.2 Quantitative evaluation of validity according to the second criterion associated with the trabecular orientation

Figures 5 and 6 show the dependence of the two introduced scalar statistics (the deviation δ of a stimulus S_{sf} from its equilibrium value $S_{\mathrm{sf}}^{\mathrm{o}}$ and the magnitude of skewness $|\beta|$ of the distribution function $f(S_{\mathrm{sf}})$, respectively) on the principal stress direction $\theta_{x'}$, defined in Fig. 3(d). As shown in Fig. 5(a–d), all stimuli showed the smallest and largest δ at $\theta_{x'}$ = 0° and 90°, respectively, which satisfied the second criterion associated with trabecular orientation shown in Fig. 2(c). As shown in

Fig. 6(a, c), the mean stress σ_{m} and nonuniformity of the mean stress $\Gamma(|\sigma_{\mathrm{m}}|)$ showed the smallest magnitudes of skewness $|\beta|$ not at $\theta_{x'} = 0°$ but at $\theta_{x'} = 15°$ and 30°, respectively. Neither σ_{m} nor $\Gamma(|\sigma_{\mathrm{m}}|)$ strictly satisfied the second criterion. In contrast, as shown in Fig. 6(b, d), the mean stress gradient $|\nabla\sigma_{\mathrm{m}}|$ and nonuniformity of the mean stress gradient $\Gamma(|\nabla\sigma_{\mathrm{m}}|)$ showed the smallest $|\beta|$ at $\theta_{x'} = 0°$, in which the principal stress directions corresponded with the principal axes of the cancellous model. Both $|\nabla\sigma_{\mathrm{m}}|$ and $\Gamma(|\nabla\sigma_{\mathrm{m}}|)$ satisfied the second criterion associated with the trabecular orientation. Furthermore, as shown in Fig. 6(d), $\Gamma(|\nabla\sigma_{\mathrm{m}}|)$ exhibited the largest $|\beta|$ at $\theta_{x'} = 90°$, in which the principal stress directions are supposed to be most deviated from the principal axes of the cancellous model due to the symmetry of the applied stress condition shown in Fig. 3(c, d). These results suggest that $\Gamma(|\nabla\sigma_{\mathrm{m}}|)$ has the highest validity among the four remodeling stimuli S_{sf}, which was compatible with the evaluation according to the first criterion.

3.3 The spatial distribution of the remodeling stimuli on the trabecular surface

In addition to the quantitative evaluation according to the two criteria, in this section, the response to change in mechanical states is discussed for each proposed model (S_{sf}: the mean stress σ_{m}, the mean stress gradient $|\nabla\sigma_{\mathrm{m}}|$, nonuniformity of the mean stress $\Gamma(|\sigma_{\mathrm{m}}|)$, and nonuniformity of the mean stress gradient $\Gamma(|\nabla\sigma_{\mathrm{m}}|)$). Figure 7 shows the spatial distribution of each remodeling stimulus S_{sf} and its bone formation/resorption regions on the trabecular surface under two different principal stress directions ($\theta_{x'} = 0°$ and 90°). As shown in Fig. 7(a–d), different principal stress directions $\theta_{x'}$ resulted in different distributions of S_{sf} and its bone formation/resorption regions, for all stimuli S_{sf}. All proposed models have the potential to respond to changes in mechanical states.

By comparing the global and local uniformity models, as shown in Fig. 7(a, c), σ_{m} (global) and $\Gamma(|\sigma_{\mathrm{m}}|)$ (local) exhibited similar localization of bone formation/resorption regions on the trabecular surface under the same principal direction $\theta_{x'}$. Likewise, as shown in Fig. 7(b, d), the similarity in the localization of bone formation/resorption regions between $|\nabla\sigma_{\mathrm{m}}|$ (global) and $\Gamma(|\nabla\sigma_{\mathrm{m}}|)$ (local) was recognized. These results suggest that global and local uniformity models could exhibit similar bone adaptation behaviors.

By comparing the models with and without the differential operation ∇ of the mean stress, σ_{m} and $\Gamma(|\sigma_{\mathrm{m}}|)$, as shown in Fig. 7(a, c), exhibited clear patterns of distribution with each single bone formation/resorption region having a large area, whereas $|\nabla\sigma_{\mathrm{m}}|$ and $\Gamma(|\nabla\sigma_{\mathrm{m}}|)$ exhibited patterns with small bone formation/resorption regions finely distributed, as shown in Fig. 7(b, d). Whether or not a remodeling stimulus S_{sf} includes the differential operation ∇ could result in different bone adaptation behaviors.

4 Discussion

In this study, we proposed novel macroscopic models of bone remodeling that assume four possible remodeling stimuli considering the microscopic mechanism of osteocytic mechanosensing. As shown in Figs. 4, 5, and 6, quantitative evaluation showed that $\Gamma(|\nabla\sigma_{\mathrm{m}}|)$ has the highest validity among the four remodeling stimuli, according to the introduced criteria based on biological rationales associated with the trabecular volume and orientation at remodeling equilibrium. Furthermore, the adaptive potential of each stimulus was discussed based on the spatial distribution of a remodeling stimulus on the trabecular surface. As shown in Fig. 7(a–d), all proposed models have the potential to respond to changes in mechanical states. Comparing (a**)** and (b) with (c) and (d) in Fig. 7, the global and local

uniformity models could exhibit similar bone adaptation behaviors. In the comparison between models with (Fig. 7(b, d)) and without (Fig. 7(a, c)) the differential operation ∇ of the mean stress, whether or not a remodeling stimulus S_{sf} includes the differential operation ∇ could result in different bone adaptation behaviors.

The models based on the uniformity of the mean stress (σ_{m} and $\Gamma(|\sigma_{\mathrm{m}}|)$) assume that σ_{m} attains a spatially uniform value at the equilibrium state, and its gradient $\nabla\sigma_{\mathrm{m}}$ thereby becomes zero, which means that the rate of the interstitial fluid flow due to daily activity could be zero in average at the equilibrium state. In contrast, the models based on the uniformity of the mean stress gradient ($|\nabla\sigma_{\mathrm{m}}|$ and $\Gamma(|\nabla\sigma_{\mathrm{m}}|)$) assume that $|\nabla\sigma_{\mathrm{m}}|$ attains a spatially uniform value at the equilibrium state, which means that the interstitial fluid could flow at a spatially uniform flow rate in average. The averaged behaviors of the interstitial fluid flow in the remodeling equilibrium state should be experimentally investigated.

To construct a reliable model of bone remodeling that can predict biological behaviors for clinical use, it is important to integrate clarified microscopic findings into a macroscopic model. Computational studies have tried to combine these different scales in various ways, such as the integration of phenomenological behaviors identified through a microscale mechanistic simulation into an existing mesoscale model (Phillips et al. 2015; Villette and Phillips 2016), multiscale integration through a multistep homogenization method (Fritsch and Hellmich 2007; Scheiner et al. 2013; Colloca et al. 2014), and a combination of mesoscale neural network computation and macroscopic finite element analyses (Unger and Könke 2008; Hambli 2010, 2011; Hambli et al. 2011). These methods were based on a multiscale analytical approach, where bone structural information from microscale

analyses was combined with macroscale bone mechanical properties. In contrast, the approach taken in this study was the reduction of a model's DOF, through which essential features captured from the complex microscopic mechanisms associated with osteocytic mechanosensing were incorporated into a simple macroscopic model.

Because the reduced model that incorporates the captured microscopic features should still have the potential to simulate the macroscopic behavior of bone adaptation, we established biological criteria that a remodeling stimulus is required to meet. Tsubota and Adachi (2006) investigated the validity of macroscopic remodeling stimuli using the skewness of their distributions as a single criterion. Extending this criterion, we established our two criteria based on biological rationales associated with the trabecular volume and the orientation of the trabecular structure. Through quantitative evaluation, we showed that nonuniformity of the mean stress gradient $\Gamma(|\nabla\sigma_{\mathrm{m}}|)$, one of the proposed remodeling stimuli incorporating the microscopic mechanism of osteocytic mechanosensing, could be a reliable macroscopic remodeling stimulus that meets these biological criteria. For clinical applicability, it is significant that a reduced model is biofidelic based on biological rationales associated with bone adaptation.

For clinical use, the proposed models should be extended to describe bone pathologies. Abnormal balance in bone remodeling is recognized in various bone diseases, including osteopetrosis, Paget's disease of bone, postmenopausal osteoporosis, and secondary osteoporosis with specific causes such as rheumatoid arthritis, glucocorticoid use, and endocrine disorders (Hirayama et al. 2002; Canalis 2003; Del Fattore et al. 2008; Mosekilde 2008; Frenkel et al. 2010; Feng and McDonald 2011; Redlich and Smolen 2012). Furthermore, histomorphometric studies have suggested that morphological

abnormalities in the lacuno-canalicular porosity (Busse et al. 2010; Milovanovic et al. 2013) and the osteocyte network (van Hove et al. 2009; van Oers et al. 2015) may play important roles for impaired mechanosensing in bone pathologies. There has also been accumulating evidence of a mechanosensory role for osteocyte primary cilium and skeletal abnormalities related to these defects (Temiyasathit and Jacobs 2010; Nguyen and Jacobs 2013). In the proposed macroscopic models, these bone pathologies, which can be regarded as a deterioration in temporal and spatial sensitivities to mechanical stimuli, would be described by variations of either the remodeling rate constant or the sensing distance l_{L}. The model variations described by these temporal and spatial parameters should be validated for each bone pathology by comparison with experimental findings.

For further validation of our study, future works should analyze bone samples from various anatomical sites under various stress conditions. In such analyses, to apply not arbitrary but reasonable stress conditions to the different samples, it is necessary to estimate mechanical states (e.g., stress and strain) unique to each sample, because the trabecular architecture adapts to its local mechanical states in each anatomical site. However, the estimation of mechanical states in different anatomical sites is a difficult problem. For a reasonable estimation in this study, we harvested the sample from the femoral head, because its mechanical states are qualitatively clear due to its characteristic morphology and can be reasonably estimated. As the next step, a method for estimating different reasonable stress conditions unique to different anatomical sites should be determined.

Moreover, morphological changes in the trabecular structure through a remodeling simulation by the proposed models should be validated. The models in this study were evaluated according to the criterion associated with the trabecular orientation considering Wolff's law. Through a remodeling

simulation, it is necessary to validate the models according to other trabecular morphometries (e.g., trabecular thickness and spacing). In addition, although the feature of fluid pressure in the lacuno-canalicular porosity was incorporated as the mean stress of the bone matrix, theoretical consideration should be given as to how the mean stress in the simple elastic model is related to the fluid pressure in the poroelastic model (Kameo et al. 2009).

In conclusion, we theoretically evaluated four possible remodeling stimuli that capture the essential microscopic features of osteocytic mechanosensing. We established criteria for quantitative evaluation based on biological rationales of bone adaptation that a macroscopic model should meet. According to the criteria, nonuniformity of the mean stress gradient $\Gamma(|\nabla\sigma_{\mathrm{m}}|)$ was shown to have high validity. We believe that the theoretical evaluation of a remodeling stimulus based on biological rationales would contribute to the establishment of a clinically applicable and reliable simulation model of bone remodeling.

Acknowledgements

This work was partially supported by the Advanced Research and Development Programs for Medical Innovation from the Japan Agency for Medical Research and Development (AMED-CREST).

References

Aarden EM, Burger EH, Nijweide PJ (1994) Function of osteocytes in bone. J Cell Biochem 55:287–299. doi: 10.1002/jcb.240550304

Adachi T, Kameo Y, Hojo M (2010) Trabecular bone remodelling simulation considering osteocytic response to fluid-induced shear stress. Philos T R Soc A 368:2669–2682. doi: 10.1098/rsta.2010.0073

Adachi T, Osako Y, Tanaka M, et al (2006) Framework for optimal design of porous scaffold microstructure by computational simulation of bone regeneration. Biomaterials 27:3964–3972. doi: 10.1016/j.biomaterials.2006.02.039

Adachi T, Tomita Y, Sakaue H, Tanaka M (1997) Simulation of trabecular surface remodeling based

on local stress nonuniformity. JSME Int Ser C 40:782–792.

Adachi T, Tsubota K, Tomita Y, Hollister SJ (2001) Trabecular surface remodeling simulation for cancellous bone using microstructural voxel finite element models. J Biomech Eng 123:403–409. doi: 10.1115/1.1392315

Burger EH, Klein-Nulend J (1999) Mechanotransduction in bone - role of the lacuno-canalicular network. FASEB J 13:S101–S112.

Busse B, Djonic D, Milovanovic P, et al (2010) Decrease in the osteocyte lacunar density accompanied by hypermineralized lacunar occlusion reveals failure and delay of remodeling in aged human bone. Aging Cell 9:1065–1075. doi: 10.1111/j.1474-9726.2010.00633.x

Canalis E (2003) Mechanisms of glucocorticoid-induced osteoporosis. Curr Opin Rheumatol 15:454–457. doi: 10.1097/00002281-200307000-00013

Carter DR (1984) Mechanical loading histories and cortical bone remodeling. Calcif Tissue Int 36 Suppl 1:S19–S24.

Carter DR, Fyhrie DP, Whalen RT (1987) Trabecular bone density and loading history: Regulation of connective tissue biology by mechanical energy. J Biomech 20:785–794. doi: 10.1016/0021-9290(87)90058-3

Colloca M, Blanchard R, Hellmich C, et al (2014) A multiscale analytical approach for bone remodeling simulations: Linking scales from collagen to trabeculae. Bone 64:303–313. doi: 10.1016/j.bone.2014.03.050

Cowin SC (1985) The relationship between the elasticity tensor and the fabric tensor. Mech Mater 4:137–147. doi: 10.1016/0167-6636(85)90012-2

Cowin SC, Hegedus DH (1976) Bone remodeling I: theory of adaptive elasticity. J Elast 6:313–326.

Cowin SC, Weinbaum S, Zeng Y (1995) A case for bone canaliculi generated as the anatomical potential. J Biomech 28:1281–1297. doi: 10.1016/0021-9290(95)00058-P

Del Fattore A, Cappariello A, Teti A (2008) Genetics, pathogenesis and complications of osteopetrosis. Bone 42:19–29. doi: 10.1016/j.bone.2007.08.029

Doane DP, Seward LE (2011) Measuring Skewness: A Forgotten Statistic? J Stat Educ 19:1–18. doi: 10.1.1.362.5312

Feng X, McDonald JM (2011) Disorders of bone remodeling. Sci York 6:121–145. doi: 10.1146/annurev-pathol-011110-130203.

Frenkel B, Hong A, Baniwal SK, et al (2010) Regulation of adult bone turnover by sex steroids. J Cell Physiol 224:305–310. doi: 10.1002/jcp.22159

Fritsch A, Hellmich C (2007) “Universal” microstructural patterns in cortical and trabecular, extracellular and extravascular bone materials: Micromechanics-based prediction of anisotropic elasticity. J Theor Biol 244:597–620. doi: 10.1016/j.jtbi.2006.09.013

Hambli R (2010) Application of neural networks and finite element computation for multiscale simulation of bone remodeling. J Biomech Eng 132:114502. doi: 10.1115/1.4002536

Hambli R (2011) Numerical procedure for multiscale bone adaptation prediction based on neural networks and finite element simulation. Finite Elem Anal Des 47:835–842. doi: 10.1016/j.finel.2011.02.014

Hambli R, Katerchi H, Benhamou C-L (2011) Multiscale methodology for bone remodelling simulation using coupled finite element and neural network computation. Biomech Model

Mechanobiol 10:133–45. doi: 10.1007/s10237-010-0222-x

Han Y, Cowin SC, Schaffler MB, Weinbaum S (2004) Mechanotransduction and strain amplification in osteocyte cell processes. Proc Natl Acad Sci U S A 101:16689–94. doi: 10.1073/pnas.0407429101

Hasegawa M, Adachi T, Takano-Yamamoto T (2015) Computer simulation of orthodontic tooth movement using CT image-based voxel finite element models with the level set method. Comput Methods Biomech Biomed Engin 1–10. doi: 10.1080/10255842.2015.1042463

Hirayama T, Danks L, Sabokbar A, Athanasou N (2002) Osteoclast formation and activity in the pathogenesis of osteoporosis in rheumatoid arthritis. Rheumatology (Oxford) 41:1232–1239. doi: 10.1093/rheumatology/41.11.1232

Huiskes R, Ruimerman R, van Lenthe GH, Janssen JD (2000) Effects of mechanical forces on maintenance and adaptation of form in trabecular bone. Nature 405:704–706. doi: 10.1038/35015116

Huiskes R, Weinans H, Grootenboer HJ, et al (1987) Adaptive bone-remodeling theory applied to prosthetic-design analysis. J Biomech 20:1135–1150. doi: 10.1016/0021-9290(87)90030-3

Jing D, Lu XL, Luo E, et al (2013) Spatiotemporal properties of intracellular calcium signaling in osteocytic and osteoblastic cell networks under fluid flow. Bone 53:531–540. doi: 10.1016/j.bone.2013.01.008

Kameo Y, Adachi T (2014a) Interstitial fluid flow in canaliculi as a mechanical stimulus for cancellous bone remodeling: in silico validation. Biomech Model Mechanobiol 13:851–860. doi: 10.1007/s10237-013-0539-3

Kameo Y, Adachi T (2014b) Modeling trabecular bone adaptation to local bending load regulated by mechanosensing osteocytes. Acta Mech 225:2833–2840. doi: 10.1007/s00707-014-1202-5

Kameo Y, Adachi T, Hojo M (2009) Fluid pressure response in poroelastic materials subjected to cyclic loading. J Mech Phys Solids 57:1815–1827. doi: 10.1016/j.jmps.2009.08.002

Kameo Y, Ootao Y, Ishihara M (2016) Theoretical investigation of the effect of bending loads on the interstitial fluid flow in a poroelastic lamellar trabecula. J Biomech Sci Eng 11:15–00663. doi: 10.1299/jbse.15-00663

Kufahl RH, Saha S (1990) A theoretical model for stress-generated fluid flow in the canaliculi-lacunae network in bone tissue. J Biomech 23:171–180. doi: 10.1016/0021-9290(90)90350-C

Kumar NC, Jasiuk I, Dantzig J (2011) Dissipation energy as a stimulus for cortical bone adaptation. J Mech Mater Struct 6:303–319.

Lacroix D, Chateau A, Ginebra MP, Planell JA (2006) Micro-finite element models of bone tissue-engineering scaffolds. Biomaterials 27:5326–5334. doi: 10.1016/j.biomaterials.2006.06.009

Milovanovic P, Zimmermann EA, Hahn M, et al (2013) Osteocytic canalicular networks: Morphological implications for altered mechanosensitivity. 7:7542–7551. doi: 10.1021/nn401360u

Mosekilde L (2008) Primary hyperparathyroidism and the skeleton. Clin Endocrinol (Oxf) 69:1–19. doi: 10.1111/j.1365-2265.2007.03162.x

Mullender MG, Huiskes R (1995) Proposal for the Regulatory Mechanism of Wolff's Law. J Orthop Res 13:503–512. doi: 10.1002/jor.1100130405

Nguyen AM, Jacobs CR (2013) Emerging role of primary cilia as mechanosensors in osteocytes. Bone 54:196–204. doi: 10.1016/j.bone.2012.11.016

Phillips AT, Villette CC, Modenese L (2015) Femoral bone mesoscale structural architecture prediction using musculoskeletal and finite element modelling. Int Biomech 2:43–61. doi: 10.1080/23335432.2015.1017609

Redlich K, Smolen JS (2012) Inflammatory bone loss: pathogenesis and therapeutic intervention. Nat Rev Drug Discov 11:234–250. doi: 10.1038/nrd3669

Reina-Romo E, Gómez-Benito MJ, Sampietro-Fuentes A, et al (2011) Three-dimensional simulation of mandibular distraction osteogenesis: Mechanobiological analysis. Ann Biomed Eng 39:35–43. doi: 10.1007/s10439-010-0166-4

Ruimerman R, Hilbers P, van Rietbergen B, Huiskes R (2005) A theoretical framework for strain-related trabecular bone maintenance and adaptation. J Biomech 38:931–941. doi: 10.1016/j.jbiomech.2004.03.037

Scheiner S, Pivonka P, Hellmich C (2013) Coupling systems biology with multiscale mechanics, for computer simulations of bone remodeling. Comput Methods Appl Mech Eng 254:181–196. doi: 10.1016/j.cma.2012.10.015

Sharma GB, Debski RE, McMahon PJ, Robertson DD (2010) Effect of glenoid prosthesis design on glenoid bone remodeling: Adaptive finite element based simulation. J Biomech 43:1653–1659. doi: 10.1016/j.jbiomech.2010.03.004

Swan CC, Lakes RS, Brand R a, Stewart KJ (2003) Micromechanically based poroelastic modeling of fluid flow in Haversian bone. J Biomech Eng 125:25–37. doi: 10.1115/1.1535191

Temiyasathit S, Jacobs CR (2010) Osteocyte primary cilium and its role in bone mechanotransduction. Ann N Y Acad Sci 1192:422–428. doi: 10.1111/j.1749-6632.2009.05243.x

Tsubota K, Adachi T (2005) Spatial and temporal regulation of cancellous bone structure: characterization of a rate equation of trabecular surface remodeling. Med Eng Phys 27:305–11. doi: 10.1016/j.medengphy.2004.09.013

Tsubota K, Adachi T (2006) Simulation study on local and integral mechanical quantities at single trabecular level as candidates of remodeling stimuli. J Biomech Sci Eng 1:124–135. doi: 10.1299/jbse.1.124

Tsubota K, Adachi T, Tomita Y (2002) Functional adaptation of cancellous bone in human proximal femur predicted by trabecular surface remodeling simulation toward uniform stress state. J Biomech 35:1541–1551. doi: 10.1016/S0021-9290(02)00173-2

Tsubota K, Suzuki Y, Yamada T, et al (2009) Computer simulation of trabecular remodeling in human proximal femur using large-scale voxel FE models: Approach to understanding Wolff's law. J Biomech 42:1088–1094. doi: 10.1016/j.jbiomech.2009.02.030

Unger JF, Könke C (2008) Coupling of scales in a multiscale simulation using neural networks. Comput Struct 86:1994–2003. doi: 10.1016/j.compstruc.2008.05.004

van Hove RP, Nolte PA, Vatsa A, et al (2009) Osteocyte morphology in human tibiae of different bone pathologies with different bone mineral density - Is there a role for mechanosensing? Bone 45:321–329. doi: 10.1016/j.bone.2009.04.238

van Oers RFM, Wang H, Bacabac RG (2015) Osteocyte Shape and Mechanical Loading. Curr Osteoporos Rep 13:61–66. doi: 10.1007/s11914-015-0256-1

van Rietbergen B, Weinans H, Huiskes R, Odgaard A (1995) A new method to determine trabecular bone elastic properties and loading using micromechanical finite-element models. J Biomech 28:69–81. doi: 10.1016/0021-9290(95)80008-5

Villette CC, Phillips AT (2016) Informing phenomenological structural bone remodelling with a mechanistic poroelastic model. Biomech Model Mechanobiol 15:69–82. doi: 10.1007/s10237-015-0735-4

Weinbaum S, Cowin SC, Zeng Y (1994) A model for the excitation of osteocytes by mechanical loading-induced bone fluid shear stresses. J Biomech 27:339–360. doi: 10.1016/0021-9290(94)90010-8

Whitehouse WJ (1974) The quantitative morphology of anisotropic trabecular bone. J Microsc 101:153–168. doi: 10.1111/j.1365-2818.1974.tb03878.x

Wolff J (1869) Ueber die bedeutung der architectur der spongiösen substanz für die frage vom knochenwachsthum. ZBT Med Wiss 223–234.

Wolff J (1892) Das gesetz der transformation der knochen. Hirschwald, Berlin

Xia SL, Ferrier J (1992) Propagation of a calcium pulse between osteoblastic cells. Biochem Biophys Res Commun 186:1212–1219. doi: 10.1016/S0006-291X(05)81535-9

Figures

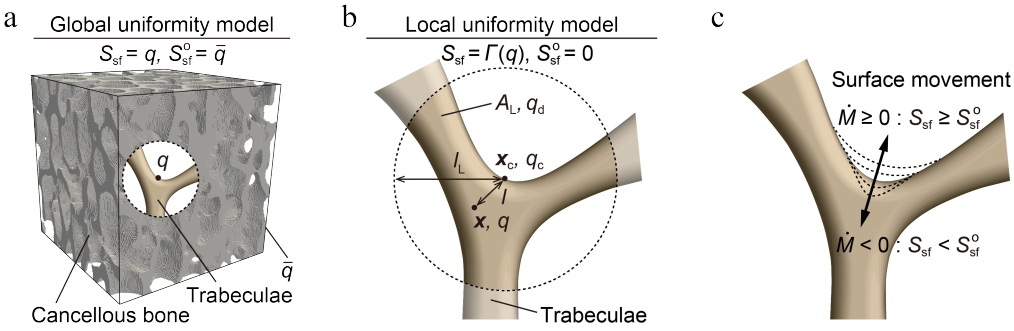

Fig. 1 Simulation models of bone remodeling. **a** In the global uniformity models, bone remodeling is driven by referring to the equilibrium value S^{o}_{sf} that is globally set by $S^{o}_{sf} = \bar{q}$. **b** In the local uniformity models, bone remodeling is driven by local nonuniformity of a mechanical quantity $\Gamma(q)$ on the trabecular surface. Considering its definition ($\Gamma(q) = \ln(q_c/q_d)$), the equilibrium value S^{o}_{sf} is locally determined by $\Gamma = 0$, because $q_c = q_d$ in the equilibrium state. **c** To determine morphological changes in the trabeculae resulting from a remodeling stimulus S_{sf}, the rate of surface movement $\dot{M}(S_{sf})$ was introduced. The rate $\dot{M}$ satisfies $\dot{M} < 0$ for $S_{sf} < S^{o}_{sf}$ and $\dot{M} \geq 0$ for $S_{sf} \geq S^{o}_{sf}$

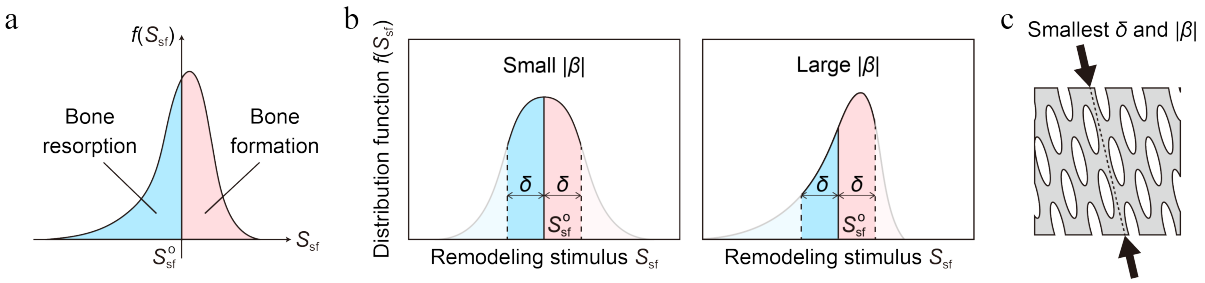

Fig. 2 Quantitative evaluation of the validity of the remodeling stimulus S_{sf}. **a** A distribution function $f(S_{sf})$ of the remodeling stimulus S_{sf}, in which bone is formed when $S_{sf} \geq S_{sf}^{o}$ and resorbed when $S_{sf} < S_{sf}^{o}$, where S_{sf}^{o} denotes a stimulus at a state of remodeling equilibrium. **b** The magnitude of skewness $|\beta|$ of the distribution function $f(S_{sf})$ was introduced as the first criterion for the validity of the remodeling stimulus S_{sf}. The magnitude of skewness $|\beta|$ was defined in the vicinity of the equilibrium state, which is determined by the averaged deviation δ of the remodeling stimulus S_{sf} from its equilibrium value S_{sf}^{o}. A small magnitude of skewness $|\beta|$, which represents a nearly symmetric distribution function $f(S_{sf})$, indicates the validity of the stimulus S_{sf}. **c** Dependence of the averaged deviation δ of the remodeling stimulus S_{sf} from its equilibrium value S_{sf}^{o} and the magnitude of skewness $|\beta|$ on the principal stress direction was introduced as the second criterion for the validity of the remodeling stimulus S_{sf}. If δ and $|\beta|$ take their minimum values under the given principal stresses along the principal axes of the trabecular structure, the validity of the stimulus S_{sf} is ensured

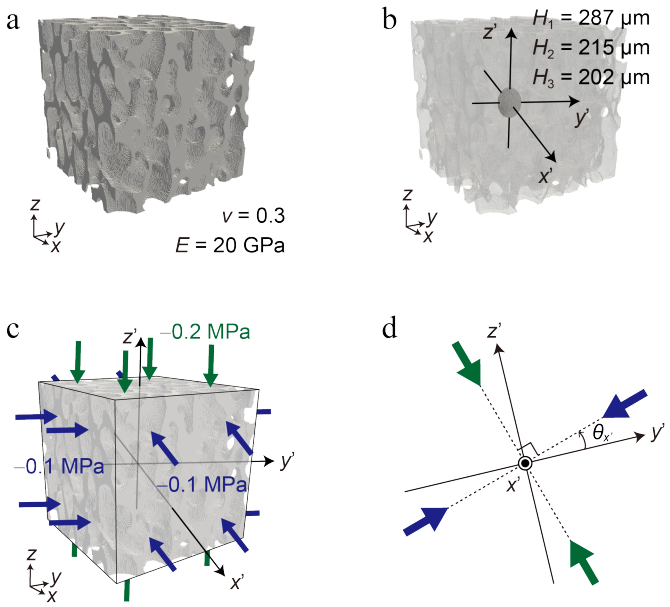

Fig. 3 A cancellous model with boundary conditions. **a** A 3D image-based finite element model of cancellous bone from a swine femoral head was developed using X-ray micro-computed tomography. **b** The fabric ellipsoid representing the trabecular orientation of the cancellous model was obtained. The principal values of the fabric tensor $\boldsymbol{H}$ were defined as H_1, H_2, and H_3 in descending order. It was assumed that the largest compressive stress was imposed along the principal axis corresponding to the largest principal value H_1, which was set as the z'-axis. The other two principal axes corresponding to H_2 and H_3 were set as the x'-axis and y'-axis, respectively. **c** Uniform compressive stresses of -0.2 MPa along the z'-axis and -0.1 MPa along the x'-axis and y'-axis were applied. **d** The principal stress directions were rotated with respect to the x'-axis. Angle $\theta_{x'}$ denotes the principal stress direction rotated from the reference condition

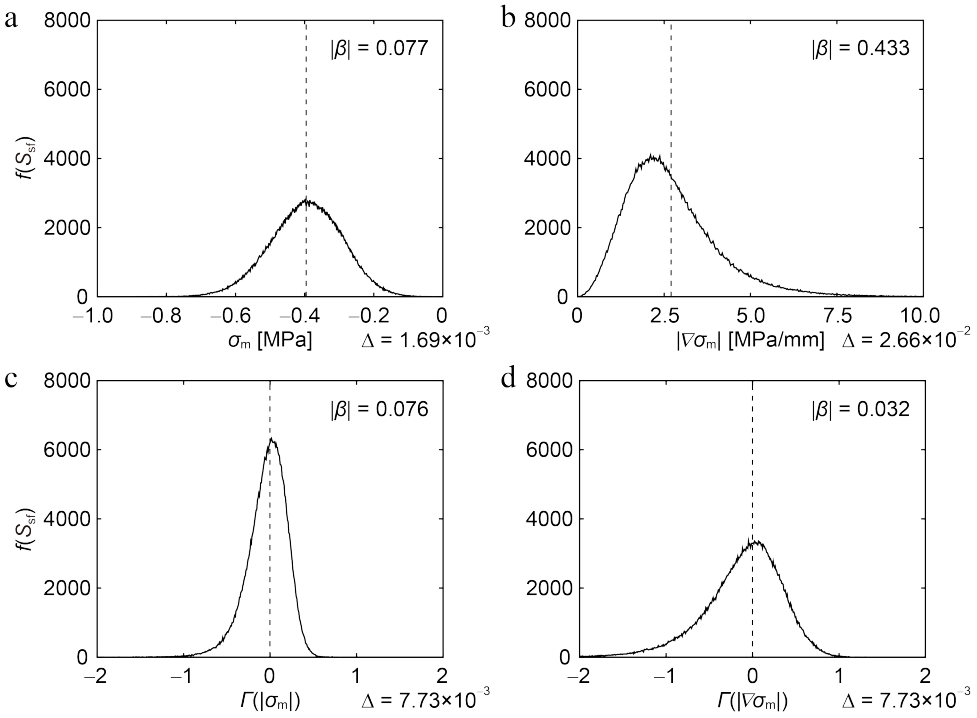

Fig. 4 The distribution function $f(S_{sf})$ and its magnitude of skewness $|\beta|$ for each remodeling stimulus S_{sf}. **a** The mean stress σ_m. **b** The mean stress gradient $|\nabla\sigma_m|$. **c** Nonuniformity of the mean stress $\Gamma(|\sigma_m|)$. **d** Nonuniformity of the mean stress gradient $\Gamma(|\nabla\sigma_m|)$. Broken lines show the equilibrium value for each remodeling stimulus. The value Δ shows the class width of each remodeling stimulus. Nonuniformity of the mean stress gradient $\Gamma(|\nabla\sigma_m|)$ showed the smallest value of the magnitude of skewness among the four remodeling stimuli ($|\beta| = 0.032$)

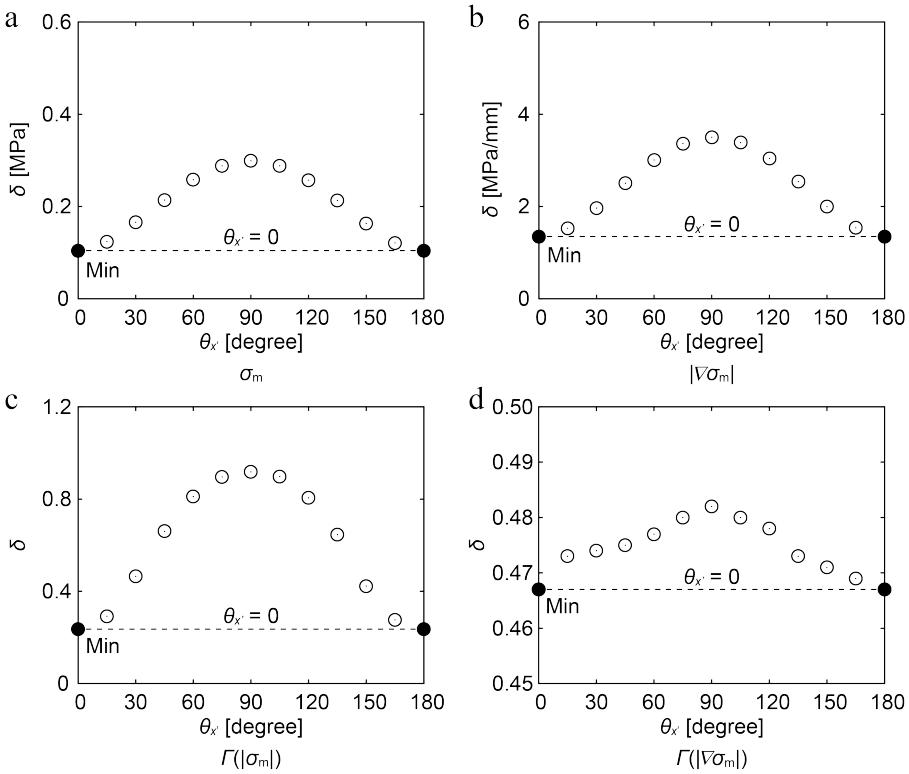

Fig. 5 Dependence of the deviation δ of a remodeling stimulus S_{sf} from its equilibrium value on the principal stress direction $\theta_{x'}$. **a** The mean stress σ_{m}. **b** The mean stress gradient $|\nabla\sigma_{\mathrm{m}}|$. **c** Nonuniformity of the mean stress $\Gamma(|\sigma_{\mathrm{m}}|)$. **d** Nonuniformity of the mean stress gradient $\Gamma(|\nabla\sigma_{\mathrm{m}}|)$. The averaged deviation δ of a remodeling stimulus was plotted against the principal stress direction $\theta_{x'}$ for each stimulus. Solid circles show the minimum values of δ. The horizontal broken line indicates the value of the averaged deviation δ at $\theta_{x'} = 0°$. All stimuli showed the smallest and largest δ at $\theta_{x'} = 0°$ and 90°, respectively

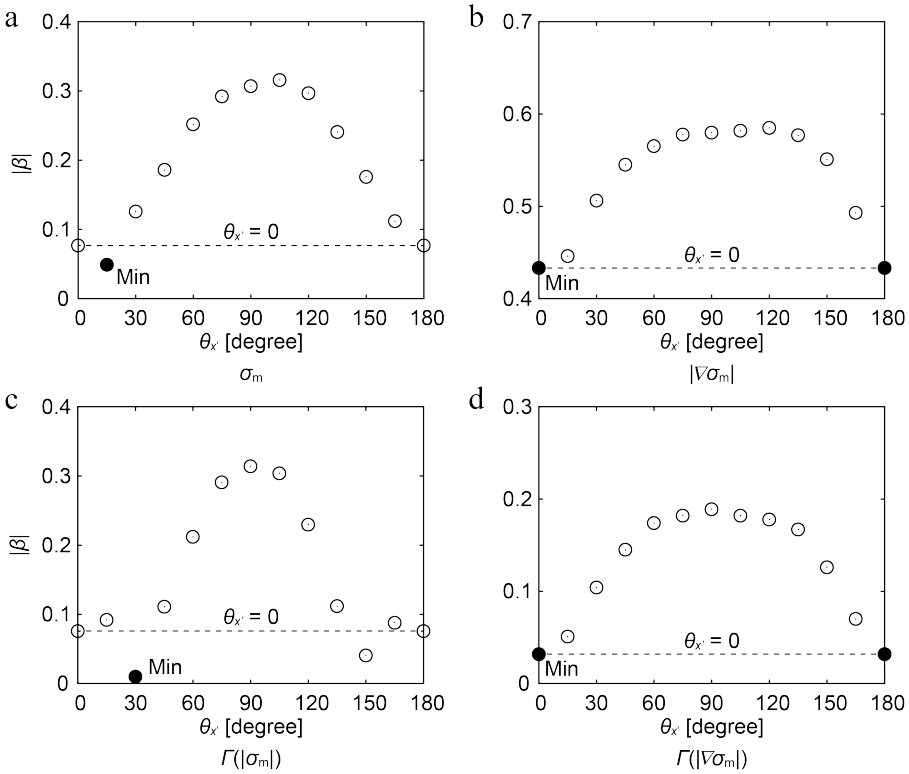

Fig. 6 Dependence of the magnitude of skewness $|\beta|$ on the principal stress direction $\theta_{x'}$. **a** The mean stress σ_{m}. **b** The mean stress gradient $|\nabla\sigma_{\mathrm{m}}|$. **c** Nonuniformity of the mean stress $\Gamma(|\sigma_{\mathrm{m}}|)$. **d** Nonuniformity of the mean stress gradient $\Gamma(|\nabla\sigma_{\mathrm{m}}|)$. Magnitudes of skewness $|\beta|$ were plotted against the principal stress direction $\theta_{x'}$ for each remodeling stimulus. Solid circles show the minimum values of $|\beta|$. The horizontal broken line indicates the value of the magnitude of skewness $|\beta|$ at $\theta_{x'} = 0°$. The mean stress gradient $|\nabla\sigma_{\mathrm{m}}|$ and nonuniformity of the mean stress gradient $\Gamma(|\nabla\sigma_{\mathrm{m}}|)$ showed the smallest $|\beta|$ at $\theta_{x'} = 0°$

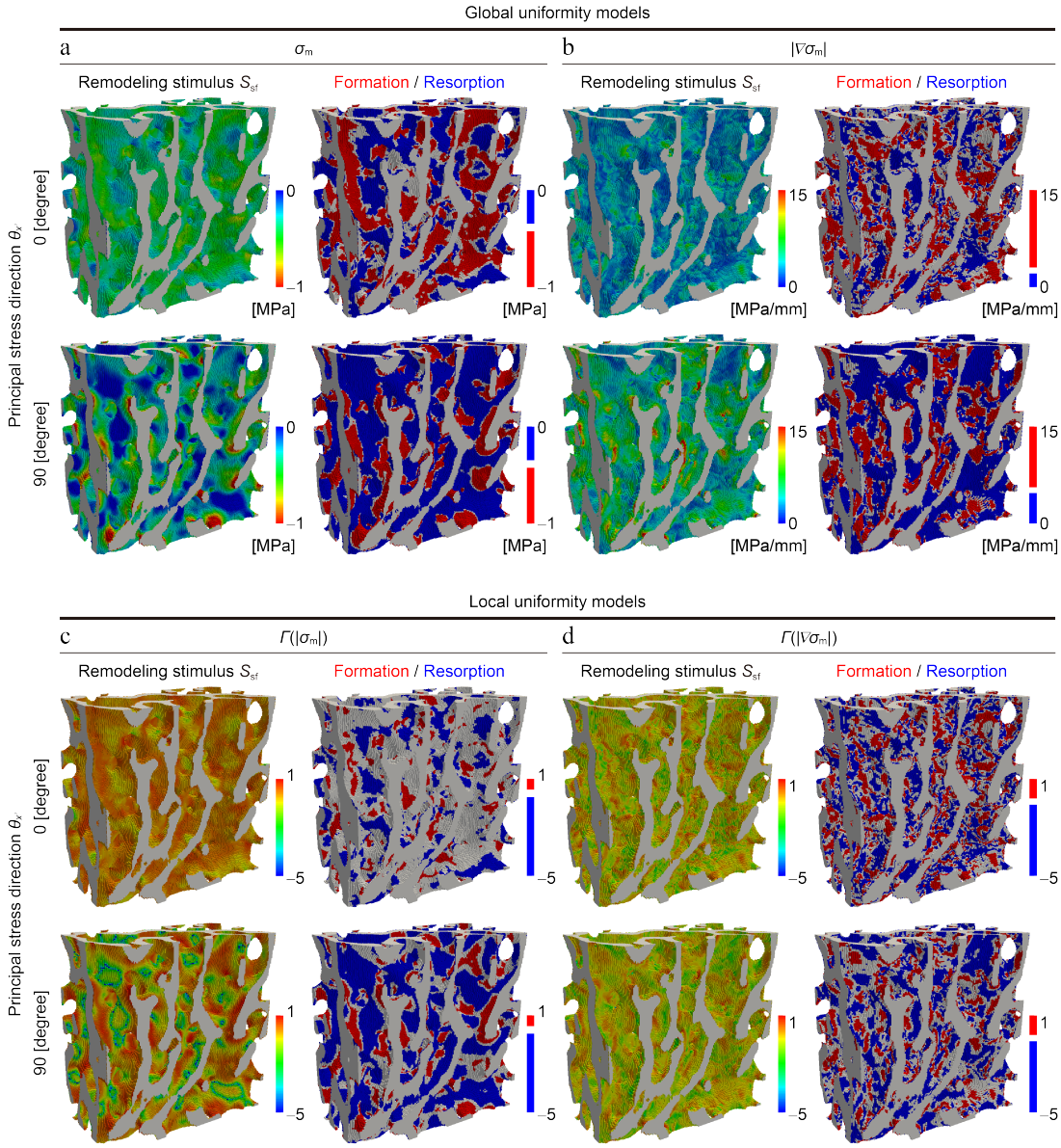

Fig. 7 Spatial distribution of the remodeling stimuli S_{sf} on the trabecular surface. **a** The mean stress σ_m. **b** The mean stress gradient $|\nabla\sigma_m|$. **c** Nonuniformity of the mean stress $\Gamma(|\sigma_m|)$. **d** Nonuniformity of the mean stress gradient $\Gamma(|\nabla\sigma_m|)$. The equilibrium zone was determined by the length of the white band in the colorbar with its ratio to the total length for both $\theta_{x'}$ (0° and 90°) corresponding for each remodeling stimulus S_{sf}. Different $\theta_{x'}$ resulted in different distributions of S_{sf} and its bone formation/resorption regions for all remodeling stimuli S_{sf}. Comparing (**a**) σ_m and

(**b**) $|\nabla\sigma_{\mathrm{m}}|$ with (**c**) $\Gamma(|\sigma_{\mathrm{m}}|)$ and (**d**) $\Gamma(|\nabla\sigma_{\mathrm{m}}|)$, the global ($\sigma_{\mathrm{m}}$, $|\nabla\sigma_{\mathrm{m}}|$) and local ($\Gamma(|\sigma_{\mathrm{m}}|)$, $\Gamma(|\nabla\sigma_{\mathrm{m}}|)$) uniformity models exhibited similar distributions of bone formation/resorption regions. Focusing on the effect of the differential operation ∇, (**a**) σ_{m} and (**c**) $\Gamma(|\sigma_{\mathrm{m}}|)$ exhibited clear patterns of distribution with each single bone formation/resorption region having a large area, whereas (**b**) $|\nabla\sigma_{\mathrm{m}}|$ and (**d**) $\Gamma(|\nabla\sigma_{\mathrm{m}}|)$ exhibited patterns with small bone formation/resorption regions finely distributed